Electromagnetic Analysis of the EAST 4-Strap ICRF Antenna with HFSS Code*

QIN Chengming (秦成明)[1], ZHANG Xinjun (张新军)[1], ZHAO Yanping (赵燕平)[1],
WAN Baonian (万宝年)[1], Franz BRAUN[2], WANG Lei (王磊)[1],
YANG Qingxi (杨庆喜)[1], YUAN Shuai (袁帅)[1], CHENG Yan (程艳)[1],
ICRF team on EAST

[1]Institute of Plasma Physics, Chinese Academy of Sciences, Hefei 230031, China
[2]Max-Planck Institute for Plasma Physics, Garching, Germany

Abstract A new ICRF antenna has been designed in EAST, whose aims are to reduce the parallel RF electric fields $E_{\|}$ and to investigate the current drive using the fast magnetosonic wave. This antenna consists of four toroidally spaced radiating straps. The electrical characteristics of the new antenna are estimated by using a three-dimensional electromagnetic commercial code. The S-parameters, RF current distribution and electromagnetic field distribution on and near the 4-strap antenna are analyzed, and the RF potentials influenced by antenna phasing and radial position are investigated.

Keywords: ICRF, RF sheaths, EAST, antenna modeling

PACS: *52.50.Qt, 52.40.Fd*

DOI: 10.1088/1009-0630/17/2/12

(Some figures may appear in colour only in the online journal)

1 Introduction

ICRF heating plays an important role in many existing fusion experiments and is considered to be one of the most promising technologies for heating future fusion devices. ICRF antennas are key components of RF heating systems for handling and delivering high power to the plasma. However, high-voltage sheaths formed on the surface of antennas and limiters can lead to RF-specific impurity production, hot spots, edge power dissipation and other unwanted effects [1−3]. These negative effects are accumulated over a discharge and hinder proper operation of future steady-state ICRF antennas.

In previous ICRF heating experiments at EAST, it was found that there was no clear heating on electrons or ions nor any production of metal impurities during an RF pulse. The dissipated RF power goes into the SOL and possibly increases the voltage across the dc-rectified sheaths, which leads to sputtering of the material surface [4,5]. A leading candidate for enhanced RF sheaths is parallel electric field generated in the near field of the antenna [6]. A new ICRF antenna has been designed for reducing the parallel electric field $E_{\|}$ and investigating the current drive by fast wave in EAST.

In this paper, the calculations of electromagnetic field and scattering parameters using 3-D HFSS simulation code [7] are carried out based on a 4-strap ICRF antenna reference model. The RF sheath voltage defined as in Ref. [8] by integration [9] of the $E_{\|}$ component along magnetic field lines has also been evaluated by assuming a simple sheath model with independent flux tubes. These estimated values are compared with the original 2-strap ICRF antenna on EAST.

2 Antenna modeling

2.1 Basic description of the antenna model

The HFSS calculations use a model with flat antenna geometry and plasma loading approximated by a sea water tank. The relative permittivity and the effective conductivity of sea water are $\varepsilon_{\mathrm{r}} = 81$ and $\sigma = 4$ S/m, respectively. However, the use of a water load instead of a plasma load does not correctly represent the slow wave fields in the plasma, since the anisotropic effect of the plasma is not included in the model. Previous measurements [10] and modelling [11] show that some information is systematically and irreversibly lost when the plasma is replaced by a dielectric. Although the water loading is isotropic, the characteristics of the near-fields are consistent with those of other codes derived from a magnetic plasma model, such as ICANT [12] and TOPICA [13].

A scheme of the antenna model is shown in Fig. 1(a).

*supported by the National Magnetic Confinement Fusion Science Program of China (No. 2015GB101001) and National Natural Science Foundation of China (Nos. 11375236 and 11375235)

The antenna is placed in a vacuum box (2.1 m × 1.5 m × 0.97 m) with radiation conditions as boundaries. In the model, the water tank (2.1 m × 1.5 m × 0.7 m) which acts as an absorber is located 2 cm in front of the antenna. The output of the HFSS code consists of arrays of real and imaginary parts of the x, y, z components of the electric field at the antenna front yz plane with 2.1 m×1.5 m dimensions. The plane is 1 cm in front of the antenna Faraday Screen (FS). In order to compare the performances of the new 4-strap antenna and the original 2-strap antenna on EAST [14], their simplified models are shown in Fig. 1(b) and (c), respectively.

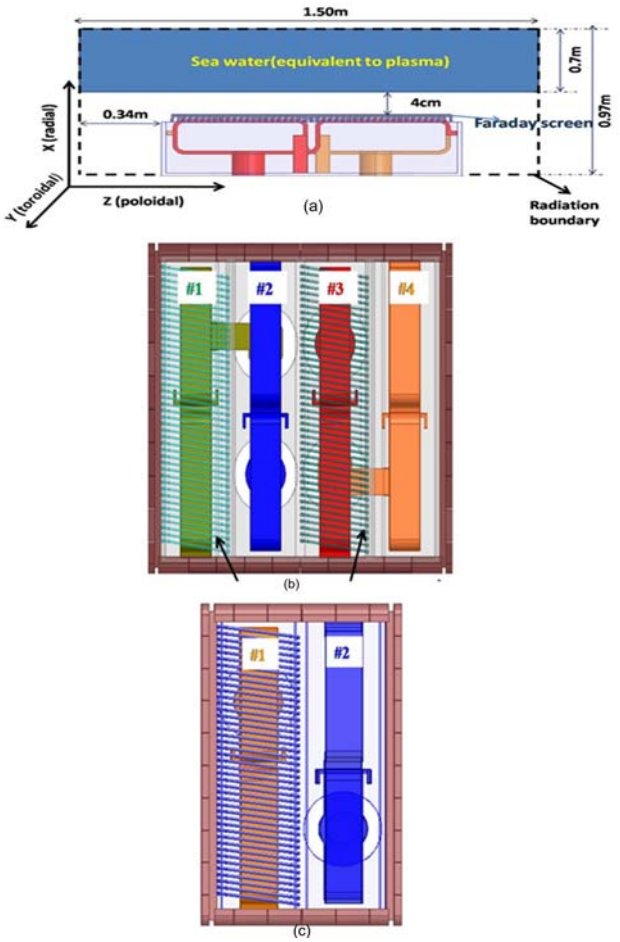

Fig.1 (a) Layout of the main distances of the 4-strap antenna model used in HFSS, (b) Simplified 4-strap antenna model, (c) Simplified original 2-strap antenna model

2.2 Analyses of the simulation results

2.2.1 S parameters

The antenna scattering (S-matrix) or impedance matrix at the location where the antenna is connected to the power system is of crucial importance to assess the compliance with power handling requirements and to design the tuning-and-matching system. The ICRF heating system is often operated at a frequency of 27 MHz in EAST, which corresponds to the H minority heating regime in deuterium plasmas [4,15]. Fig. 2 presents a comparison of the S-parameters of 2-strap antenna and 4-strap antenna. It is shown that the S-parameters of the 4-strap antenna are improved compared with that of the 2-strap antenna at frequency of 27 MHz. However, the 4-strap antenna configuration also adds more cross-terms between straps, which renders more mutual coupling for the 4-strap array, leading to difficulties in impedance matching [16]. Thus toroidal de-couplers are necessary between straps in multiple-straps antenna array.

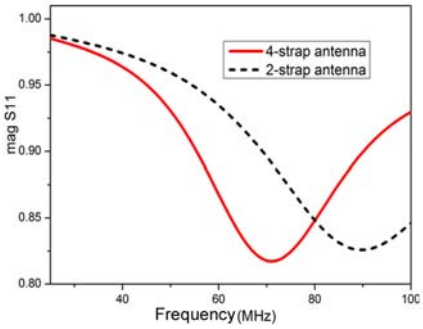

Fig.2 A comparison of the S-parameters of 2-strap antenna and 4-strap antenna on EAST

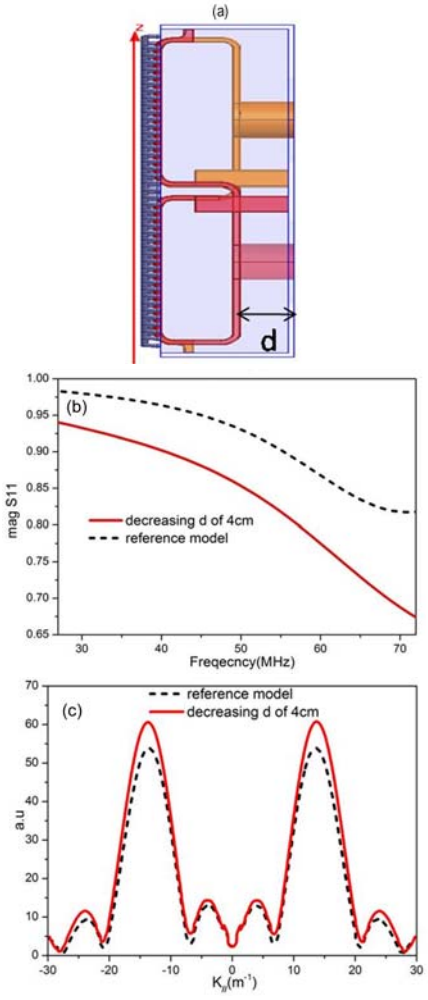

Fig.3 (a) Reducing the distance between the current-return plate and the backplate of the antenna box for improving coupling, (b) Comparison of the mag (S11) for the reference model and the optimization model, (c) Comparison of the power spectrum of the reference model and the optimization model with (0,π,0,π) phasing

To further improve the S-parameters, we optimize the distance between the current-return plate and the backplate of the antenna box (see Fig. 3(a)). In Fig. 3(b), it is shown that the S11 magnitude with a 4 cm reduction of d is lower than the reference in the frequency range 25-72 MHz due to the increase of the inductance of straps. Taking into account geometrical constraints, assembly requirements and RF quantities, an appropriate distance of d is chosen as 1 cm. Fig. 3(c) shows that a decrease of d results in an increase of the magnitude of the k-parallel spectrum in both primary peaks and sidelobes in the $(0,\pi,0,\pi)$ heating case. In addition, according to Ref. [17], the width of the straps is half of the antenna box size, which would be a good compromise between the radiated power and the mutual coupling.

2.2.2 Optimization of current straps

The RF current distribution calculated on the ICRF antenna at the $(0,\pi,0,\pi)$ phase is shown in Fig. 4(a). It is found that the RF currents are concentrated on both edges of the strap and the connected point to the lower-plate. So we can implement some slots on the straps (see Fig. 4(b)), which increase the pumping and also improve the efficiency of cooling by moving the cooling tubes from the center to the edges of the straps.

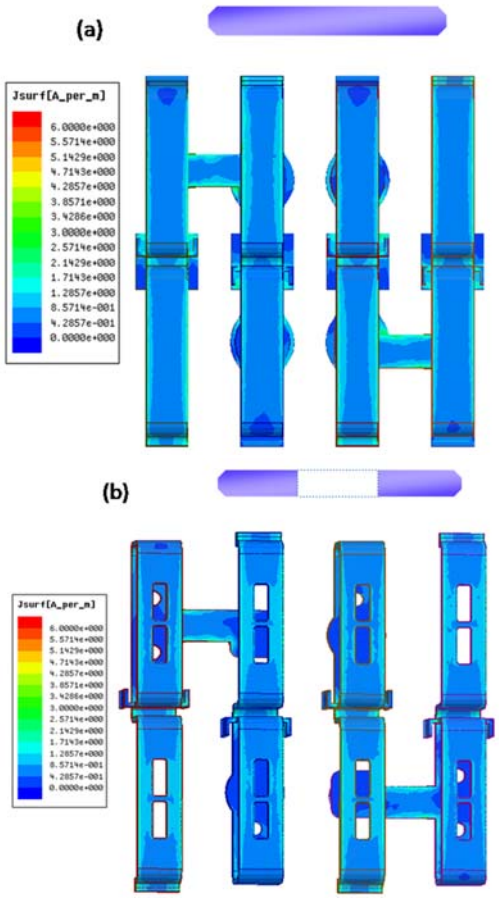

(a) Reference antenna model, (b) Optimized antenna model

Fig.4 RF currents distribution on the antenna straps with $(0,\pi,0,\pi)$ phasing

2.2.3 Antenna power spectrum

The power spectrum was evaluated for different feeding configurations. The plane for electromagnetic fields calculation was placed 1 cm in front of the antenna FS, which is an output from HFSS, one can determine the launched power spectrum. In Fig. 5(a), the 4-strap antenna configuration of the coupled power attributed to the main peak is much narrower and its height increases compared to the 2-strap antenna. Mostly, dipole phasing operations are used because the coupled power components near $k_{\|}$=0 are reduced which leads to increased absorption in the plasma. In Fig. 5(b), the power spectrum for 2-strap antennas with a $\pi/2$ phase angle has a large full width half maximum of the primary peak compared to the 4-strap antenna with a (0, $\pi/2$, 0, $3\pi/2$) phase. It is clear that the primary peak becomes narrower and its height increases while all the secondary lobes are suppressed by increasing the number of antenna straps [18]. In general, for a given RF frequency, different antenna phasings (leading to different $k_{\|}$ spectra excited) are expected to show different coupling properties. Fig. 5(c) shows the power spectra

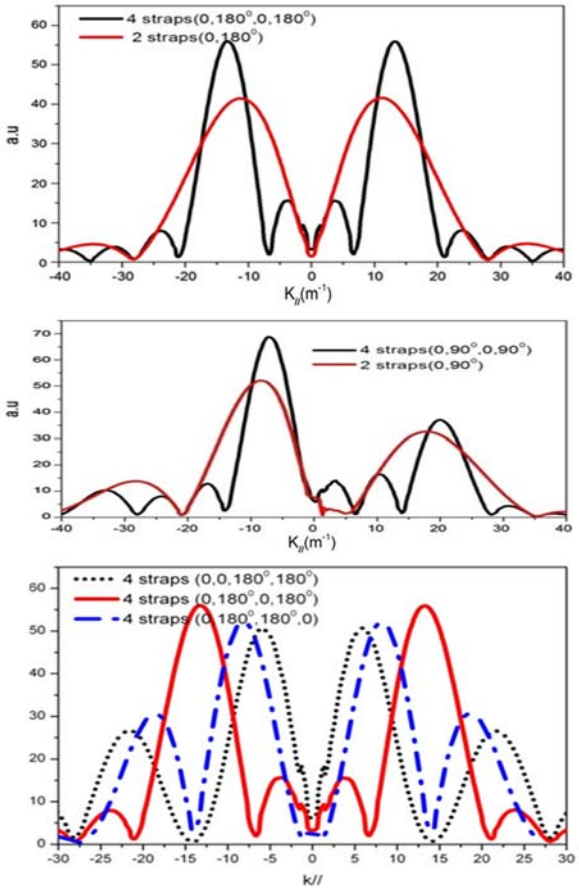

Fig.5 (a) Comparison of the power spectra for 4-strap antenna with $(0,\pi,0,\pi)$ phasing and the power spectra for the 2-strap antenna with $(0,\pi)$ phasing, (b) Comparison of the power spectra for the 4-strap antenna with $(0,\pi/2,0,3\pi/2)$ phasing and the power spectra for the 2-strap antenna with $(0,\pi/2)$ phasing, (c) Power spectra of the 4-strap antenna for $(0,0,\pi,\pi)$, $(0,\pi,0,\pi)$ and $(0,\pi,\pi,0)$ phasing

of 4-strap antennas with (0,0,π,π) (0,π,0,π) and (0,π,π,0) phases. In the case of the standard dipole configuration (0,π,0,π), roughly 80% of the power is launched around $\left|k_{\|}\right| \sim 12\ \mathrm{m}^{-1}$ and other phases have only ~55% of the power associated to lower $\left|k_{\|}\right|$ ~7 m^{-1} values. There is a trade-off between low and high parallel wave number spectra. Waves with lower $k_{\|}$ are less evanescent than waves with higher $k_{\|}$, whereas the wave absorptivity increases with $k_{\|}$. Therefore, the antenna coupling properties depend on a compromise for producing an excitation with a low enough $k_{\|}$ to ensure an acceptable plasma coupling but with a high enough $k_{\|}$ to achieve satisfactory ICRF absorption [19].

2.2.4 $E_{\|}$ and RF potentials on the antenna

The formation of RF sheaths is induced by the action of an RF field with a substantial component $k_{\|}$ parallel to the equilibrium magnetic field. In the vicinity of a material boundary, electrons are accelerated out of the plasma by $k_{\|}$ faster than the heavier ions, and a confining DC sheath potential ϕ develops to confine electrons and restore equilibrium quasineutrality [1,9]. These RF sheaths likely cause the acceleration of ions impacting on the obstacles and, consequently, enhance sputtering and localize heat flux. It was considered to be related to the ICRF antennas structure [8], and thus the $E_{\|}$ field on and near the 4-strap antenna and the RF potentials are investigated based on simple RF sheath models.

The electric fields $E_{x,y,z}$ are calculated for 1 W forward power put into each of the coaxial input planes and then re-normalized to 1 MW net power using the integral poynting vector flux. The surface for E-fields calculations was placed 1 cm in front of the antennas. According to the literature [20], RF sheaths can be minimized when the screen elements are aligned along the static magnetic field via structure symmetry and therefore the angle between FS elements and the toroidal magnetic field is designed as 8° based on the typical plasma parameters on EAST [5]. To account for a variety of possible field line connections, including those starting or ending at the limiters, the RF potentials $|V_{\mathrm{sheath}}| = \int \left|E_{\|}\right| \cdot \mathrm{d}l$ are calculated as on the magnetic field lines passing in front of the antenna at the inclination angle.

Fig. 6(a) and (b) present a comparison of imaginary E-fields for the original EAST 2-strap antenna at (0,π) phasing and the 4-strap antenna at (0,π,0,π) phasing. As one observes, the imaginary $E_{\|}$ fields for the 4-strap antenna are much lower than that for the 2-strap antenna. In addition, the positive and negative peaks of $E_{\|}$ occur at the corners of the antenna box and limiters. This is likely because the magnetic field lines are connected with the radially protruding limiters, where the electric fields are forced to be perpendicular to the protruding surfaces and gain a large parallel component. These positive and negative peaks correspond to electric fields in opposite directions on a given magnetic field line. When a magnetic field line is passing through this region, $E_{\|}$ cancellation will be largest if the positive and negative values integrate to zero. In Fig. 6(c), the voltages are plotted versus the vertical position Z along the middle septum of the antenna model. It can be seen that the peak values of $\left|V_{\|}\right|$ are approximately 30% lower for the 4-strap antenna configuration than for the 2-strap antenna geometry. The (0,π,0,π) phasing can effectively reduce the $E_{\|}$ fields and the RF potentials compared with the original 2-strap antenna at the dipole phase.

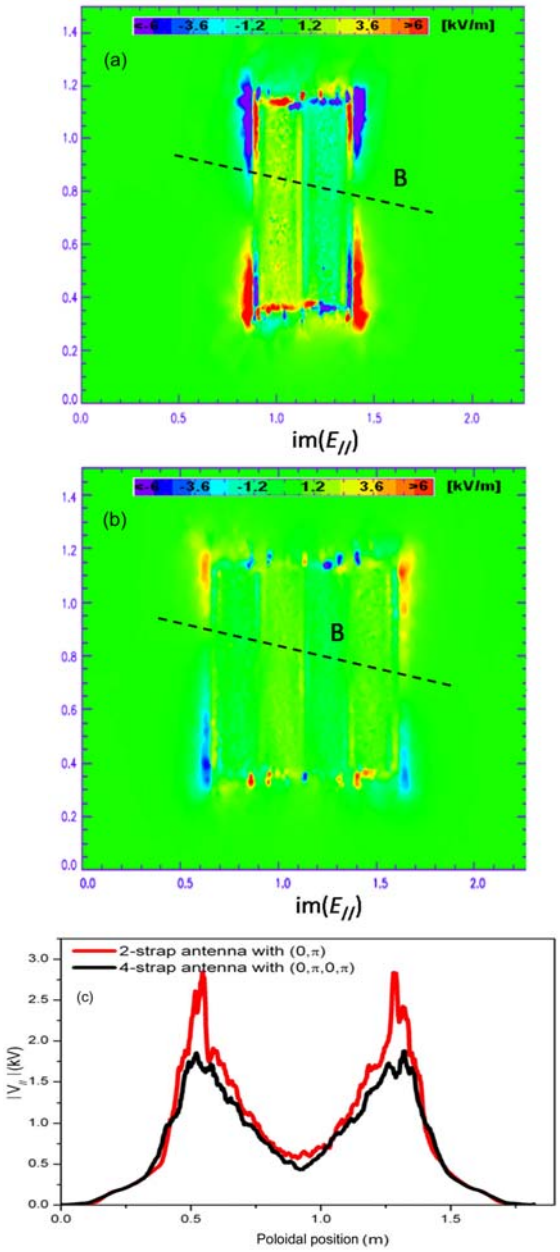

Fig.6 (a) The distribution of the imaginary part of $E_{\|}$ for the 2-strap antenna with (0,π) phasing, (b) The distribution of the imaginary part of $E_{\|}$ for the 4-strap antenna with (0,π,0,π) phasing, (c) Comparison of the RF potentials $\left|V_{\|}\right|$ versus poloidal position for the 2-strap antenna and the 4-strap antenna

Fig. 7 shows the sheath potentials at a location 1 cm in front of the 4-strap antenna as a function of the av-

eraged poloidal position along the antenna structure with different phasing. In Fig. 7, the RF potentials with (0,0,0,0) phasing are much higher than other antenna phases. This is likely because the cancellation of $E_{\|}$ along field lines is greater for dipole phasing than for monopole phasing for antenna structures which are not aligned with the equilibrium magnetic field [21]. The highest impurity production can be expected for (0,0,0,0) phasing. The peak values for (0,π,0,π) and (0,π,π,0) seem to be comparable by balancing between the (0,0,0)-phasing image current contributions. Similar results have been observed on JET [20], Tore Supra [22], TFTR [23], and ASDEX Upgrade [24].

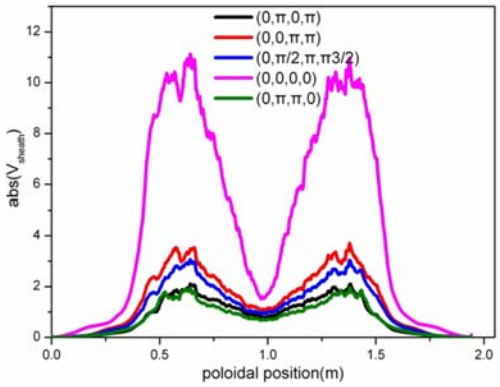

Fig.7 $|V_{\|}|$ calculated for different phasing for the 4-strap antenna configuration

In order to estimate how $|V_{\|}|$ change with increasing radial distance from the antenna, the surface was scanned to 2 mm, 5 mm and 1 cm in front of the antennas. The RF potential maps for radial distances of 2 mm, 5 mm and 1 cm are presented in Fig. 8, provided the forward voltage is 1 V at the antenna feeders. We note that $|V_{\|}|$ is reduced by increasing the radial distance. The peak values of $|V_{\|}|$ are reduced by 25% for a radial distance of 1 cm, and by 18% for the radial distance of 5 mm. We can conclude that the very intensive $E_{\|}$ are localized in the antenna vicinity. It can be reduced by putting the locations of the intersection of protruding parts with magnetic field lines further away from the antenna. In this condition, the effect of the electric fields of the antenna is lower and then the RF potentials are reduced.

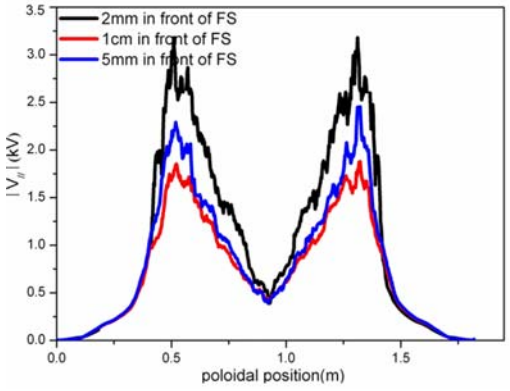

Fig.8 $|V_{\|}|$ calculated for different radial position in front of the Faraday screen

3 Summary

A new 4-strap antenna was modeled and optimized for the reduction of $E_{\|}$ fields and the improvement of current driving based on ANSYS HFSS calculations with flat antenna geometry and water load. The calculations show that with an increasing number of antenna straps, the power spectrum peak becomes narrower and its height increases while all the secondary lobes are suppressed, and thus the driving current can be increased. Typically (0,π, 0,π) and (0,π, π,0) phasing are used for heating and (0,$\pi/2$,π,$3\pi/2$) phasing is used for co-current and counter-current drive. The high $E_{\|}$ fields are located at the positions where RF limiters and antenna box corners intersect magnetic field lines. These regions with high $E_{\|}$ have also high rectified DC potentials based on the concept $|V_{\|}| = \int |E_{\|}| \cdot \mathrm{d}l$. Producing the maps of $E_{\|}$ components and $|V_{\|}|$ gives an important insight into the distribution of V_{sheath}. The RF potentials can be reduced by putting the locations of the intersection further away from the antenna, where the effect of the electric fields of the antenna is lower. A further significant reduction of such $|V_{\|}|$ can be achieved for 4-strap antennas operating at (0,π,0,π) and (0,π,π,0) phasing. Further work is needed to fully interpret the phenomena that are responsible for the impurity influx in ICRF heating experiments in machines with metallic walls, and the failure of RF power penetration into the plasma core in current drive experiments.

Acknowledgments

We would like to thank F. Braun and V. Bobkov for providing HFSS simulations and useful discussions.

References

1 Myra J R and D'Ippolito D A. 1990, Nucl. Fusion, 30: 845
2 Wukitch S J, Lipschultz B, Marmar E, et al. J. Nucl. Mater., 363-365: 491
3 Colas L, Basiuk V, Beaumont B, et al. 2006, Nucl. Fusion, 46: S500
4 Zhang X J, Zhao Y P, Mao Y Z, et al. 2011, Plasma Sci. Technol., 13: 172
5 Li Jiangang, Wan Baonian. 2011, Nucl. Fusion, 51: 094007
6 Garrett M L. 2012, Mitigation of RF Sheaths Through Design and Implementation of Magnetic Field-Aligned ICRF Antenna [Ph.D]. Massachusetts Institute of Technology, Plasma Science and Fusion Center
7 High Frequency Structure Simulator (HFSS), www.ansoft.com
8 Myra J, D'Ippolito D, Ho Y. 1996, Fusion Engineering and Design, 31: 291
9 Perkins F. 1989, Nucl. Fusion, 29: 4583
10 Pavlov I P and Heikkinen J A. 1995, Phys. Plasmas, 2: 3573

11 Swain D W, Carter M D, Wilson J R, el al. 2003, Fusion Science and Technology, 43: 503
12 Colas L, Heuraux S, Brémond S, Bosia G. 2005, Nucl. Fusion, 45: 767
13 Lancellotti V, et al. 2006, Nucl. Fusion, 46: S476
14 Qin C M, Zhao Y P, Wang H Q, et al. 2013, Plasma Phys. Control. Fusion, 55: 015004
15 Zhang X J, Zhao Y P, Wan B N, et al. 2010, 23rd IAEA Fusion Energy Conference (11-16 October 2010 Daejon, Korea), EXW/P7-30
16 Saito Kenji, Kumazawa Ryuhei, Seki Tetsuo, et al. 2010, J. Plasma Fusion Res. SERIES, 5: S2104
17 Braun F, ICRF Group. 2005, 16th AIP Conference Proceedings, 787: 238
18 Abdul Hannan. 2013, Modelling Ion Cyclotron Resonance Heating and Fast Wave Current Drive in Tokamaks [Ph.D]. Alfvén Laboratory School of Electrical Engineering KTH Royal Institute of Technology Stockholm, Sweden
19 Lerche E, Bobkov V, Jacquet P. 2009, 18th AIP Conference Proceedings, 1187: 93
20 Bures M, Jacquinot J J, Stamp M F, et al. 1992, Nucl. Fusion, 32: 1139
21 Bures M, Jacquinot J J, LAWSONM, et al. 1991, Plasma Phys. Conlroll. Fusion, 33: 37
22 Colas L, Ekedahl A, Goniche M, et al. 2007 Plasma Phys. Controll. Fusion, 49: B35
23 Stevens J E, Bush C, Colestock P L. 1990, Plasma Phys. Controll. Fusion, 32: 189
24 Bobkov V, Bilato R, Braun F, et al. 2009, AIP Conference Proceedings, 1187: 125

(Manuscript received 24 February 2014)
(Manuscript accepted 12 June 2014)
E-mail address of corresponding author
ZHANG Xinjun: xjzhang@ipp.ac.cn